Modular Kinematic Modelling of Articulated Buses

Maciej Marcin Michałek, *Senior Member, IEEE*, Bartosz Patkowski, and Tomasz Gawron, *Member, IEEE*

***Abstract*—Development of compact and easy to use mathematical models of articulated vehicles for the motion planning, control, and localization purposes becomes more and more important in the era of intelligent transportation systems, especially when there exists a need of reliable predictions of motion for multi-body (semi-)automated freight and public transportation vehicles of various kinematic structures. We propose a modular algorithmic approach to kinematic modelling of nonholonomic (multi-)articulated buses, including the N-trailer vehicles as a special case, comprising a car-like prime-mover passively interconnected with arbitrary number of segments (wagons/trailers) equipped with fixed or steerable wheels, and with various locus of a driving axle in a kinematic chain. Kinematic models are valid under an assumption of a pure rolling of all the vehicle wheels (no skid/slip motion), which is practically justified for the low-speed maneuvering conditions. The proposed approach leads to compact nonlinear models which, thanks to their modular construction, preserve clear geometrical interpretation of velocity couplings between the vehicle segments. Derivations of kinematic models for popular structures of articulated and bi-articulated urban buses are presented for various driving-axle locus and steering capabilities. Experimental model validation, conducted with a full-scale wagon-driven articulated bus, illustrates utility of the approach.**

***Index Terms*—articulated urban bus, N-trailer, kinematics, modelling for control, experimental model validation**

I. Introduction

CONTEMPORARY development of public and freight transportation leads towards the increase in demand of large capacity vehicles and urban buses, [30], [15], [4]. This trend it justified by arguments of economic savings, energy consumption conservation, and pollution level reduction caused by limiting a number of vehicles and human drivers needed for translocation of large amount of goods and people. As a consequence, manufacturers of trucks and urban buses currently design the large capacity constructions in a form of articulated and multi-articulated vehicles, see Fig. 1. Application of articulations makes the long vehicles flexible in use and admit agile maneuvering, even in cluttered (urban) environments. However, maneuvering with long articulated vehicles is difficult, burdening, and can be also dangerous, even for experienced drivers. Difficulties come, apart from a limited visibility range of a driver and substantial dimensions of a vehicle's body, from numerous specific properties characteristic to multi-body nonholonomic kinematics. The latter have been widely addressed in the literature for the case of tractor-trailer vehicles – see for example [40], [29], [18], [1], [37], [9], [43]. On the other hand, definitely less attention has been paid in the literature on kinematic modelling and analysis of the multi-body buses which admit, in contrast to more conventional tractor-trailer (or N-trailer) vehicles, more general steering and driving schemes, where a traction drive can be mounted either on a tractor or on a selected wagon unit, [6], [4]. In this sense, the N-trailers can be treated as a special case of the articulated structures. Although some modelling approaches have been proposed for the articulated buses on a dynamical level, see [7], [26], [24], [44], there is a need to develop methods for reliable modelling approaches for the (multi-)articulated vehicles and buses which would provide more compact models being simpler in the practical usage and formal analysis, and to be tractable by low-power computational units used in the embedded (on-board) automated vehicle systems, [17], [16], [35], [2]. Generic kinematic models of the multi-body vehicles, describing a low-speed geometry of their constrained (nonholonomic) motion [38], are expected to be useful in solving such problems as: formal analysis of kinematic properties [14], fast planning of nominal agile maneuvers [32], [13], [42], low-cost simulation and motion prediction of a vehicle [21], [8], [6], [22], [12], [10], feedback control and driver-assistance design for low-speed maneuvering [3], [11], [32], optimization of some construction/design parameters [36], [12], [25], as well as for embedded solutions of the control and localization tasks in the automated/intelligent vehicles [28], [19], [8], [33].

Figure 1. The articulated urban bus *Urbino 18 Electric* and the bi-articulated trolleybus *Trollino 24* produced by the Solaris Bus & Coach S.A. company.

In view of the above considerations, we propose a modular generic framework which facilitates building compact nonlinear kinematic models of the nonholonomic multi-body articulated buses and N-trailers, which (thanks to a modular structure) preserve a clear geometrical interpretation of velocity couplings between the vehicle segments. Generic nature

This work was supported in part by the National Centre for Research and Development (NCBR), Poland, as a grant No. POIR.04.01.02-00-0081/17, and in part by the research subvention No. 0211/SBAD/0911.

M. M. Michałek and T. Gawron are with the Poznan University of Technology (PUT), Institute of Automatic Control and Robotics (IAR), Poznań, Poland (e-mail: {maciej.michalek/tomasz.gawron}@put.poznan.pl).

B. Patkowski is with the Solaris Bus & Coach S.A. company, Bolechowo, Poland (e-mail: bartosz.patkowski@solarisbus.com).

and scalability of the approach admits: an arbitrary number of articulations present in a vehicle chain, fixed or steerable wheels of the vehicle's segments (wagons/trailers), a various location of a traction drive (i.e., a driven axle) in a kinematic chain, and a flexible selection of a distinguished/reference point of a vehicle. To the authors' best knowledge the methodology described in this paper, in contrast to alternative works addressing the problem of kinematic modelling of articulated vehicles (see, e.g. [43], [1], [29], [37], [32]), provides a modelling framework of a level of modularity, compactness of formulation, and admissibility of possible design options not available in the literature thus far. This paper builds upon and extends the prior conference paper [34].

According to the above arguments, the modelling concept will be basically presented for the articulated buses, since their kinematic structures are more generic (they admit a wider diversity of steering and driving schemes relative to the tractor-trailers). We will refer, however, to the special case of N-trailers where it is appropriate.

The rest of the paper is organized as follows. Section II collects all the key assumptions, introduces the configuration variables, control inputs, kinematic parameters, motion constraints, and the underlying kinematic relationships valid for the articulated vehicles under consideration. The main result in a form of the proposed modular modelling framework is presented in Section III. Application examples of the framework are provided in Section IV, where various versions of kinematic models of the articulated and bi-articulated buses are derived. Experimental validation results for the articulated electric vehicle are presented in Section V, while Section VI contains a qualitative comparison of the proposed kinematic modelling with an alternative kinetic approach to modelling. Section VII concludes the paper.

Notation: In the text, we denote: by $|\mathcal{B}|$ a cardinality of set $\mathcal{B}$, by $\emptyset$ the empty set, by $\mathbf{0}$ the zero-vector of an appropriate dimension, by $\triangleq$ the equality by definition, by $:=$ a substitution operator; we use the auxiliary vectors $\boldsymbol{c}^\top \triangleq [1\ 0]$, $\boldsymbol{d}^\top \triangleq [0\ 1]$, and we write shortly: $\mathrm{s}\alpha \equiv \sin\alpha$ and $\mathrm{c}\alpha \equiv \cos\alpha$.

II. Assumptions and Basic Relationships

A. Main assumptions

We will consider the (multi-)articulated buses which comprise the $N+1$ segments (bodies), namely, a car-like prime mover (called *tractor*) with attached the (arbitrarily large) number of N single-axle *wagons* equipped with fixed or steerable wheels, see Fig. 2. All the bus segments are interconnected in an open kinematic chain by the passive rotary joints – every one located with a non-zero offset behind an axle of a preceding segment. The kinematic modelling approach proposed in this paper is valid under the following main assumptions:

A1: Only planar motion of a bus is considered (i.e., the roll and pitch degrees of freedom are neglected).
A2: All the vehicle's wheels rotate without skid/slip effects.
A3: All the vehicle's segments are treated as rigid bodies.
A4: A number of independent kinematic control inputs of the vehicle model is equal to a total number of its degrees of freedom in a planar motion.
A5: The front effective tractor's wheel is actively steerable, the rear effective wheel is fixed; the wheels of the wagons can be either fixed or actively steerable.
A6: Only a fixed (non-steerable) wheel, either of a tractor or of a selected wagon, can be actively driven.

Assumption A1 comes from the fact that we are mainly interested in the low-speed planar maneuvers, like docking and parking, etc., with buses in a (semi-)structured workspaces. Assumption A2 is commonly formulated for the slowly moving wheeled vehicles and ensures preservation of the nonholonomic constraints in the conditions of low-speed maneuvers satisfying A1, [1], [38], [14]. Satisfaction of A2 is practically justified when maneuvers are performed on a solid ground with sufficient friction and traction forces acting between the wheels and a motion surface [21]. Under these conditions, any skid/slip effects usually do not affect a vehicle motion in a substantial manner and can be neglected, [20]. Assumption A3 allows one to neglect any flexibilities of the vehicle's bodies under the low-speed motion conditions. A4 prevents a non-uniqueness in determination of the vehicle-body velocities on a kinematic level in the planar motion conditions. Assumption A5 admits a conventional car-like tractor unit (for which, in most cases, the rear axle is fixed) and fairly general constructions of the multi-body vehicle in the context of its steering capabilities. In the articulated buses, one usually avoids steering of those wheels which are driven by actuators.

B. Vehicle's configuration, parameters, inputs, and constraints

A single-track kinematic structure of a multi-articulated vehicle is presented in Fig. 2. The vehicle's segments are numbered by $i = 0, 1, \ldots, N$; the tractor is a segment number 0, while the last wagon is a segment number N. Every segment is characterized by two kinematic parameters: the segment length $L_i > 0$ and the hitching offset $L_{hi} > 0$ (only positive offsets are present in the articulated buses, in contrast to tractor-trailer vehicles, [1], [9]). The effective wheels of wagons can be fixed or actively steerable. Let us introduce a set of indexes, $\mathcal{I}_s \subseteq \{1, \ldots, N\}$, containing indexes of

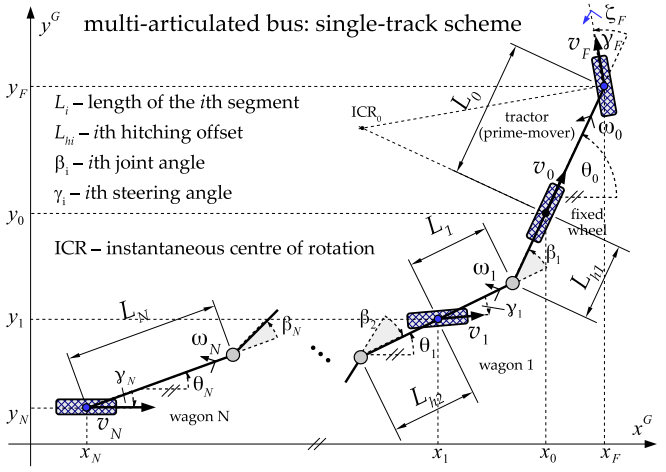

Figure 2. A single-track kinematic structure of a multi-articulated bus comprising a tractor and the N wagons with (possibly) steerable wheels.

those wagons which have steerable wheels. A configuration of the articulated vehicle can be uniquely determined by the following variables:

- a steering angle of a tractor's effective steering wheel
$$\gamma_F \in \mathcal{Q}_F \triangleq [-\bar{\gamma}_F; \bar{\gamma}_F], \quad \bar{\gamma}_F \in (0; \pi/2), \tag{1}$$
where $\bar{\gamma}_F$ comes from a limited mechanical range of a pivoting motion of the effective steering wheel,
- a pose of a *distinguished* jth segment, $j \in \{0, 1, \ldots, N\}$,
$$\boldsymbol{q}_j \triangleq [\theta_j \ x_j \ y_j]^\top = [\theta_j \ \boldsymbol{p}_j^\top]^\top \in \mathbb{S}^1 \times \mathbb{R}^2, \tag{2}$$
comprising the orientation angle θ_j of a segment body, and the position $\boldsymbol{p}_j$ of a midpoint of its wheels' axle,
- the N joint angles ($i = 1, \ldots, N$)
$$\beta_i \triangleq (\theta_{i-1} - \theta_i) \in \mathcal{Q}_B \triangleq [-\bar{\beta}_i, \bar{\beta}_i], \ \bar{\beta}_i \in (0; \pi/2), \tag{3}$$
where $\bar{\beta}_i$ comes from an admissible mechanical range of the joint angle between the segments i and $i-1$,
- a number of $S = |\mathcal{I}_s|$ steering angles of actively steerable wagon wheels ($0 \leq S \leq N$)
$$\gamma_s \in \mathcal{Q}_s \triangleq [-\bar{\gamma}_s; \bar{\gamma}_s], \quad \bar{\gamma}_s \in (0; \pi/2), \quad s \in \mathcal{I}_s. \tag{4}$$

We can collect the configuration variables in a vector
$$\boldsymbol{q} \triangleq [\gamma_F \ \beta_1 \ \ldots \ \beta_N \ \boldsymbol{\gamma}_s^\top \ \boldsymbol{q}_j^\top]^\top \in \mathcal{Q}, \tag{5}$$
where $\boldsymbol{\gamma}_s$ is the S-dimensional vector of wagon steering angles, $\dim(\boldsymbol{q}) = 4 + N + S$, and $\mathcal{Q} = \mathcal{Q}_F \times \mathcal{Q}_B^N \times \mathcal{Q}_s^S \times \mathbb{S}^1 \times \mathbb{R}^2$.

Remark 1: In general, the distinguished segment, of a pose represented by (2), can be chosen arbitrarily. However, in particular applications of a model, one may select the distinguished segment upon specific needs, for example: as a guiding segment of a vehicle (if the segment is crucial for the motion control or planning objectives), as a measurement segment (if the segment carries sensors providing a vehicle's localization or feedback signals), as a reference segment (if the segment is crucial for a synchronization with some external system or for a motion performance assessment), etc.

Let us denote by ω_i and v_i, $i = 0, \ldots, N$, respectively, an angular velocity of the ith vehicle's segment and a longitudinal velocity of a mid-point $\boldsymbol{p}_i$ of the effective wheel belonging to the ith segment, see Fig. 2. The velocity v_0 relates to a (fixed) rear effective wheel of a tractor. Introducing a motion curvature
$$\kappa_i \triangleq \omega_i / v_i \tag{6}$$
of the ith segment, and recalling the well-known relation $\omega_0 = (v_0/L_0)\tan\gamma_F$ for the car-like kinematics, one observes that the bounded set $\mathcal{Q}_F$ defined in (1) limits a maximal admissible absolute motion curvature of a tractor segment:
$$\forall\, t \geq 0 \ \ |\kappa_0(t)| \leq \bar{\kappa}_0 = (\tan\bar{\gamma}_F)/L_0. \tag{7}$$

Furthermore, by assumptions A2 and A5, the following motion constraints must be satisfied:
$$\begin{aligned} &\dot{x}_F \sin(\theta_0 + \gamma_F) - \dot{y}_F \cos(\theta_0 + \gamma_F) = 0, \\ &\dot{x}_i \sin(\theta_i + \gamma_i) - \dot{y}_i \cos(\theta_i + \gamma_i) = 0, \\ &r\xi_F = v_F, \quad r\xi_i = v_i, \quad i = 0, 1, \ldots, N, \end{aligned} \tag{8}$$
where r is the (effective) radius of a wheel (assuming the same radii for all the wheels of a vehicle), whereas ξ_F and ξ_i are the angular speeds, respectively, of the tractor's effective steering wheel and the ith segment's effective wheel ($\gamma_i \equiv 0$ if the ith wheel is non-steerable). Under assumptions A2 and A5, kinematics of an articulated bus is represented by $S + N + 4$ configuration variables and has (upon (8)) $N + 2$ nonholonomic constraints imposed. The first two constraints in (8) express the requirement of zeroing the sums of all the velocity components projected on the directions perpendicular to the planes of particular wheels (the constraints commonly defined for the nonholonomic wheeled vehicles, [29], [1], [5]). Thus, on a kinematic level, the total number of degrees of freedom of a bus is equal to $S + N + 4 - (N + 2) = S + 2$. Therefore, only $S+2$ independent kinematic control inputs can be selected for this kind of vehicle (this result quantitatively complements the assumption A4).

Independent control inputs of the (multi-)articulated bus include

- steering rates of the steering wheels:
$$\zeta_F \in \mathcal{U}_F \triangleq [-\bar{\zeta}_F; \bar{\zeta}_F] \quad \text{for a tractor,} \tag{9}$$
$$\zeta_s \in \mathcal{U}_s \triangleq [-\bar{\zeta}_s; \bar{\zeta}_s], \ s \in \mathcal{I}_s \quad \text{for wagons,} \tag{10}$$
- a single driving longitudinal velocity
$$v_k \in \mathcal{U}_v \triangleq [-\bar{v}; \bar{v}] \tag{11}$$
of a driven axle of the kth vehicle's segment,

where $\bar{\zeta}_F, \bar{\zeta}_s, \bar{v} \in (0, \infty)$ are the upper kinematic control bounds imposed either by properties of the actuators or, more conservatively, by motion safety conditions. As a consequence, the available $(2 + S)$-component kinematic control input of a multi-articulated bus takes the following general form
$$\boldsymbol{u} \triangleq \begin{bmatrix} \zeta_F \\ \boldsymbol{\zeta}_s \\ v_k \end{bmatrix} \in \mathcal{U} \triangleq \mathcal{U}_F \times \underbrace{\mathcal{U}_s \times \ldots \times \mathcal{U}_s}_{S \text{ times}} \times \mathcal{U}_v, \tag{12}$$
where $\boldsymbol{\zeta}_s = [\zeta_s : s \in \mathcal{I}_s]^\top$ is the S-dimensional vector of the steering rates for all the effective wagon wheels which are actively steerable.

Remark 2: A selection of the index k, introduced in (11), is not arbitrary – it depends on a vehicle's driving scheme. Various driving schemes are used in practical constructions of buses (see Section IV).

C. Underlying kinematic relationships in a modular form

We will determine a set of underlying kinematic relationships which are useful to formulate the kinematic modelling approach of the articulated buses in a modular form.

Using the steering rates introduced in (9), one can directly write the steering kinematics
$$\dot{\gamma}_F = \zeta_F, \qquad \dot{\gamma}_s = \zeta_s, \quad s \in \mathcal{I}_s, \tag{13}$$
recalling (upon assumption A5) that $\gamma_0 \equiv 0$, thus $\{0\} \notin \mathcal{I}_s$.

Next, upon the kinematic scheme presented in Fig. 3, explaining the geometric projections of velocity components on the ith passive joint ($i = 1, \ldots, N$), one can easily derive (see

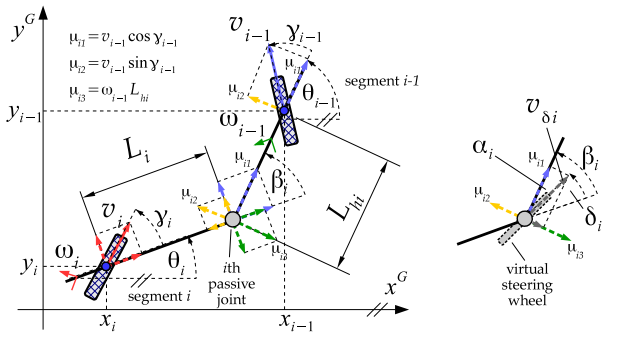

Figure 3. A kinematic structure of an articulated kinematic pair with steerable wheels explaining velocity components projected on the joint and the concept of a virtual steering wheel located in the joint (see [1]).

also [37], [9]) the following velocity transformation between any two neighbouring vehicle's segments:

$$\underbrace{\begin{bmatrix}\omega_i\\ v_i\end{bmatrix}}_{\boldsymbol{u}_i} = \underbrace{\begin{bmatrix} -\frac{L_{hi}}{L_i}\frac{\mathrm{c}(\beta_i-\gamma_i)}{\mathrm{c}\gamma_i} & \frac{\mathrm{s}(\beta_i-\gamma_i+\gamma_{i-1})}{L_i\,\mathrm{c}\gamma_i} \\ L_{hi}\frac{\mathrm{s}\beta_i}{\mathrm{c}\gamma_i} & \frac{\mathrm{c}(\beta_i+\gamma_{i-1})}{\mathrm{c}\gamma_i}\end{bmatrix}}_{\boldsymbol{J}_i(\beta_i,\gamma_i,\gamma_{i-1})} \underbrace{\begin{bmatrix}\omega_{i-1}\\ v_{i-1}\end{bmatrix}}_{\boldsymbol{u}_{i-1}}, \tag{14}$$

where $\boldsymbol{u}_i$ and $\boldsymbol{u}_{i-1}$ are the vectors of (pseudo-)velocities, respectively, of the ith and $(i-1)$st segments, while $\boldsymbol{J}_i(\beta_i,\gamma_i,\gamma_{i-1})$ is a velocity transformation matrix. An inverse of this matrix takes the form

$$\boldsymbol{J}_i^{-1}(\beta_i,\gamma_i,\gamma_{i-1}) = \begin{bmatrix} -\frac{L_i}{L_{hi}}\frac{\mathrm{c}(\beta_i+\gamma_{i-1})}{\mathrm{c}\gamma_{i-1}} & \frac{\mathrm{s}(\beta_i-\gamma_i+\gamma_{i-1})}{L_{hi}\mathrm{c}\gamma_{i-1}} \\ L_i\frac{\mathrm{s}\beta_i}{\mathrm{c}\gamma_{i-1}} & \frac{\mathrm{c}(\beta_i-\gamma_i)}{\mathrm{c}\gamma_{i-1}}\end{bmatrix}. \tag{15}$$

Remark 3: It is evident upon (14) and (15) that the transformation matrix $\boldsymbol{J}_i(\beta_i,\gamma_i,\gamma_{i-1})$ is well determined for all $\beta_i \in [-\pi,\pi)$ if only $|\gamma_i| < \pi/2$, while the inverse matrix $\boldsymbol{J}_i^{-1}(\beta_i,\gamma_i,\gamma_{i-1})$ is well determined for all $\beta_i \in [-\pi,\pi)$ if $L_{hi} \neq 0$ and $|\gamma_{i-1}| < \pi/2$. Since in the articulated buses holds $L_{hi} > 0$ for all i, the only restricting conditions concern the steering angles which in all practical constructions are satisfied.

Let us introduce two auxiliary vectors $\boldsymbol{c}^\top \triangleq [1\ 0]$ and $\boldsymbol{d}^\top \triangleq [0\ 1]$, and an auxiliary matrix

$$\boldsymbol{\Gamma}_i(\beta_i,\gamma_i,\gamma_{i-1}) \triangleq \boldsymbol{I} - \boldsymbol{J}_i(\beta_i,\gamma_i,\gamma_{i-1}),$$

where $\boldsymbol{I} \in \mathbb{R}^{2\times 2}$ is an identity matrix. Now, we can write $\omega_i = \boldsymbol{c}^\top \boldsymbol{u}_i$ and $v_i = \boldsymbol{d}^\top \boldsymbol{u}_i$. By time-differentiation of (3) one can express the joint-angle kinematics as follows

$$\begin{aligned}\dot\beta_i &= \omega_{i-1} - \omega_i = \boldsymbol{c}^\top [\boldsymbol{u}_{i-1} - \boldsymbol{u}_i] \\ &\overset{(14)}{=} \boldsymbol{c}^\top [\boldsymbol{J}_i^{-1}(\beta_i,\gamma_i,\gamma_{i-1}) - \boldsymbol{I}]\boldsymbol{u}_i \\ &= \boldsymbol{c}^\top \boldsymbol{\Gamma}_i(\beta_i,\gamma_i,\gamma_{i-1})\boldsymbol{J}_i^{-1}(\beta_i,\gamma_i,\gamma_{i-1})\boldsymbol{u}_i, \end{aligned} \tag{16}$$

which is valid for $i = 1,\dots,N$.

To extend the concept of virtual steering wheels (see [1]), let us introduce a virtual steering angle $\delta_i \triangleq (\beta_i - \alpha_i) \in (-\pi/2;\pi/2)$ of a virtual steering wheel located at the ith passive joint as depicted in Fig. 3. The virtual steering wheel determines an instantaneous direction of a resultant longitudinal velocity $v_{\delta i}$ of the ith rotary joint. By elementary geometric arguments, one can verify upon Fig. 3 that

$$\delta_i = \beta_i - \arctan\left(\frac{L_{hi}\kappa_{i-1}}{\cos\gamma_{i-1}} - \tan\gamma_{i-1}\right), \tag{17}$$

where κ_{i-1} is a motion curvature of the $(i-1)$st segment (cf. (6)). Having the virtual steering angle (17) and the velocity $v_{\delta i}$, one can express $\omega_i = (v_{\delta i}\sin\delta_i - v_i\sin\gamma_i)/L_i$ (see Fig. 3) which, under the constraint $v_{\delta i}\cos\delta_i - v_i\cos\gamma_i = 0$ resulting from assumption A3, allows expressing the curvature κ_i defined by (6) as dependent only on angles, that is,

$$\kappa_i = \frac{\cos\gamma_i}{L_i}(\tan\delta_i - \tan\gamma_i) = \frac{\sin(\delta_i-\gamma_i)}{L_i\,\cos\delta_i}. \tag{18}$$

The above formula remains valid for $i = 1,\dots,N$; for $i = 0$ a motion curvature of the tractor's body reduces to the well known relation (cf. (7))

$$\kappa_0(\gamma_F) = \frac{1}{L_0}\tan\gamma_F. \tag{19}$$

Observing that $\delta_i = \delta_i(\beta_i,\gamma_{i-1},\kappa_{i-1})$, and after combining (18) with (17), one derives a recursive formula for a motion curvature of the ith segment, i.e.,

$$\kappa_i(\beta_i,\gamma_i,\gamma_{i-1},\kappa_{i-1}) = \frac{\sin(\delta_i(\beta_i,\gamma_{i-1},\kappa_{i-1}) - \gamma_i)}{L_i\,\cos\delta_i}. \tag{20}$$

which, after a substitution to the right-hand side of (20) the terms $\kappa_{i-1} = \kappa_{i-1}(\beta_{i-1},\gamma_{i-1},\gamma_{i-2},\kappa_{i-2}),\dots,\kappa_1 = \kappa_1(\beta_1,\gamma_1,0,\kappa_0)$ together with (19), leads to the form $\kappa_i(\gamma_F,\beta_1,\dots,\beta_i,\gamma_1,\dots,\gamma_i)$ expressed solely with the joint angles and the steering angles of the successive segments, beginning from the tractor and finishing on the ith segment. As a consequence, and recalling definition (6), the velocity vector $\boldsymbol{u}_i$ introduced in (14) can be expressed in the form

$$\boldsymbol{u}_i = \begin{bmatrix}\kappa_i(\beta_1,\dots,\beta_i,\gamma_F,\gamma_1,\dots,\gamma_i)\\ 1\end{bmatrix} v_i, \tag{21}$$

where $\gamma_l \equiv 0$ for any index $1 \le l \le i$ such that $l \notin \mathcal{I}_s$.

Remark 4: Expressing κ_i in the form (20) is beneficial because one can avoid singularities of (6), in the case of zero velocities, and its potential numerical sensitivity in the case of a very slow motion of a vehicle. On the other hand, (20) is bounded only if $|\delta_i| < \pi/2$; this constraint usually delimits from above an admissible maximal absolute value of $|\beta_i|$ by some upper bound $b_i > 0$. However, if $b_i \ge \bar\beta_i$ (see (3)), such a limitation does not impose any new practical constraints – in this context, the reader is referred also to Remark 8 in Section IV.

The last relationship, needed for the purposes of modelling, is the kinematics of any jth rigid body of a vehicle satisfying constraints (8), which can be represented by the unicycle-like model:

$$\dot{\boldsymbol{q}}_j \triangleq \begin{bmatrix}\dot\theta_j\\ \dot x_j\\ \dot y_j\end{bmatrix} = \underbrace{\begin{bmatrix}\boldsymbol{c}^\top\\ \boldsymbol{d}^\top\cos(\theta_j+\gamma_j)\\ \boldsymbol{d}^\top\sin(\theta_j+\gamma_j)\end{bmatrix}}_{\boldsymbol{G}(\theta_j,\gamma_j)} \underbrace{\begin{bmatrix}\omega_j\\ v_j\end{bmatrix}}_{\boldsymbol{u}_j}, \tag{22}$$

where $\gamma_j \equiv 0$ if $j \notin \mathcal{I}_s$ (note: $\gamma_0 \equiv 0$ by assumption A5).

III. Modular Modelling Framework

Having derived the basic relationships (13), (16), (14), (22), and (21), one can formulate the modular approach to kinematic modelling of articulated vehicles after selecting (as input data to the algorithm):

- a number of articulations, N, present in a vehicle chain,
- the axles of wagons equipped with steerable wheels,
- a vehicle's distinguished segment (a tractor or one of the wagons),
- a location of a driving axle (the rear tractor's axle or an axle of one of the wagons with non-steerable wheels).

The modelling algorithm consists of the following steps:

S1: Select the set of indexes $\mathcal{I}_s$ corresponding to the wagons' axles with actively steerable wheels. Formulate the steering kinematics (13).

S2: For $i := 1$ to N derive the joint kinematics (16) taking $\gamma_i \equiv 0$ if $i \notin \mathcal{I}_s$.

S3: Select an index j of the distinguished vehicle's segment with pose (2), and write its body-kinematics (22) using the index j. Take $\gamma_j \equiv 0$ if $j \notin \mathcal{I}_s$.

S4: Select an index k of the driving axle and the driving velocity v_k; express all the velocity vectors $\boldsymbol{u}_i$ and $\boldsymbol{u}_j$ appearing, respectively, in steps S2 and S3 with the velocity $\boldsymbol{u}_k = [\omega_k \; v_k]^\top$ applying the transformation (14) or its inverse.

S5: Express the velocity $\boldsymbol{u}_k$ in the resultant equations obtained in step S4 in the form (21) using the curvatures (20) and (19).

S6: Collect the steering kinematics from step S1, the joint kinematics from step S2, and kinematics of the distinguished segment from step S3 (the latter two expressed with the velocity $\boldsymbol{u}_k$) into the resultant driftless dynamical system

$$\dot{\boldsymbol{q}} = \boldsymbol{S}(\boldsymbol{q})\boldsymbol{u} \tag{23}$$

with configuration (5) and control input (12), where $\dim(\boldsymbol{S}) = (4 + N + S) \times (2 + S)$ and $S = |\mathcal{I}_s|$.

Remark 5: In most practical applications (except, e.g., some articulated fire trucks), the steering inputs ζ_s (for $s \in \mathcal{I}_s$) are directly related to other configuration variables of a vehicle by some feedback control functions, e.g. $\zeta_s = \zeta_s(\boldsymbol{q})$, usually designed in order to automatically decrease the so-called maximal off-track of a cornering vehicle, see e.g. [19], [16]. In this case, only a two-component vector $\boldsymbol{u} = [\zeta_0 \; v_k]^\top$ remains to the user disposal as an independent kinematic control input in (23).

Remark 6: In the contemporary constructions of articulated buses, the driving axle can be located either on a prime-mover or on a wagon, thus $k \in \{0, \ldots, N\}$. However, in the case of typical tractor-trailer (N-trailer) vehicles, the driven axle is usually located on a tractor, that is, $k = 0$.

Remark 7: Sometimes, more than only one axle is driven in a chain of an articulated vehicle in order to improve effectiveness of traction forces generation. However in such a case, still only a single axle is driven independently, while the other ones must be synchronized with this *reference driving-axle* to satisfy assumptions A2-A4. The index k, which has to be selected in step S4, should indicate just this reference driving-axle.

IV. Examples

In this section, we provide several derivation examples of kinematic models for the two most popular articulated bus structures used in a public transportation today: a two-body bus with a single articulation (in two versions of a driving axle locus), and a bi-articulated three-body bus.

A. Derivation of models for a bus with a single articulation

Figure 4 presents two possible structures of a two-body articulated bus ($N = 1$): the so-called *pushing articulated bus* (or *pusher*, [6], [15], [4]), where the wagon's axle is driven ($k = 1$) but is non-steerable ($\mathcal{I}_s = \emptyset$), and the so-called *pulling articulated bus* (or *puller*, [6], [15]), where the driven axle is located on the tractor segment ($k = 0$) but the wagon's axle is steerable ($\mathcal{I}_s = \{1\}$).

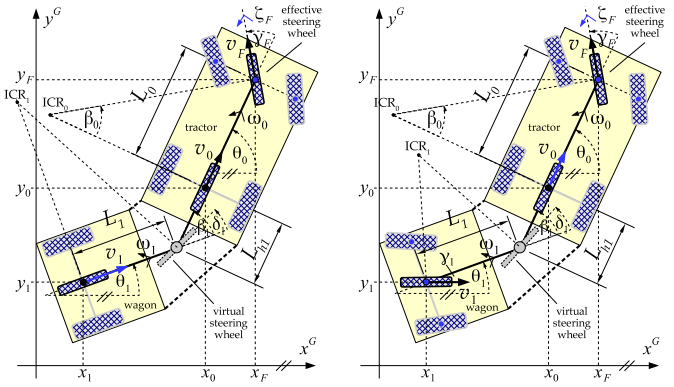

Figure 4. Kinematic structures of buses with a single articulation: the *pusher* (left) with a driven but non-steerable wagon axle, and the *puller* (right) with a non-driven but steerable wagon axle; kinematic control inputs are highlighted in blue for both structures.

1) Modelling a pushing bus with a fixed wagon wheel: Let us go through the particular design steps.

Step S1: Since $\mathcal{I}_s = \emptyset$, we write only

$$\dot{\gamma}_F = \zeta_F. \tag{24}$$

Step S2: For $i = 1 = N$ we have

$$\dot{\beta}_1 = \boldsymbol{c}^\top \boldsymbol{\Gamma}_1(\beta_1, 0, 0)\boldsymbol{J}_1^{-1}(\beta_1, 0, 0)\boldsymbol{u}_1, \tag{25}$$

where

$$\boldsymbol{J}_1^{-1}(\beta_1, 0, 0) = \begin{bmatrix} -\frac{L_1}{L_{h1}}\mathrm{c}\beta_1 & \frac{1}{L_{h1}}\mathrm{s}\beta_1 \\ L_1\mathrm{s}\beta_1 & \mathrm{c}\beta_1 \end{bmatrix} \tag{26}$$

is the inverse transformation matrix (15) in a reduced form obtained for $\gamma_1 = \gamma_0 \equiv 0$.

Step S3: If the wagon is a distinguished segment we take $j = 1$, thus

$$\dot{\boldsymbol{q}}_1 \overset{(22)}{=} \boldsymbol{G}(\theta_1, 0)\boldsymbol{u}_1, \qquad \boldsymbol{q}_1 = [\theta_1 \; x_1 \; y_1]^\top, \tag{27}$$

since $\gamma_1 \equiv 0$.

Step S4: For the *pushing* articulated bus we have to select $k = 1$, determining v_1 as a longitudinal-velocity input of a model. Since $\boldsymbol{u}_1 = [\omega_1 \; v_1]^\top$ is already present in the formulas derived in steps S2-S3, there is no need here to use the transformation (14).

Step S5: We express

$$\boldsymbol{u}_1 = \begin{bmatrix} \kappa_1(\gamma_F,\beta_1) \\ 1 \end{bmatrix} v_1, \tag{28}$$

with the curvature reduced in this case to (see (20) and (17))

$$\kappa_1(\beta_1,\gamma_F) = \frac{1}{L_1}\tan\underbrace{\left(\beta_1 - \arctan\left(\frac{L_{h1}}{L_0}\tan\gamma_F\right)\right)}_{\delta_1(\beta_1,\gamma_F)}. \tag{29}$$

Step S6: By collecting the formulas (24), (25), and (27), and by replacing $\boldsymbol{u}_1$ with (28), one obtains the following kinematic model (the zero arguments of matrices have been omitted for compactness)

$$\underbrace{\begin{bmatrix} \dot\gamma_F \\ \dot\beta_1 \\ \dot{\boldsymbol{q}}_1 \end{bmatrix}}_{\dot{\boldsymbol{q}}} = \underbrace{\begin{bmatrix} 1 & 0 \\ 0 & \boldsymbol{c}^\top\boldsymbol{\Gamma}_1(\beta_1)\boldsymbol{J}_1^{-1}(\beta_1)\begin{bmatrix}\kappa_1(\gamma_F,\beta_1)\\1\end{bmatrix} \\ \boldsymbol{0} & \boldsymbol{G}(\theta_1)\begin{bmatrix}\kappa_1(\gamma_F,\beta_1)\\1\end{bmatrix} \end{bmatrix}}_{\boldsymbol{S}(\boldsymbol{q})\in\mathbb{R}^{5\times 2}} \underbrace{\begin{bmatrix}\zeta_F\\ v_1\end{bmatrix}}_{\boldsymbol{u}} \tag{30}$$

$$= \begin{bmatrix} 1 & 0 \\ 0 & -\left(1+\frac{L_1}{L_{h1}}\mathrm{c}\beta_1\right)\kappa_1(\gamma_F,\beta_1)+\frac{1}{L_{h1}}\mathrm{s}\beta_1 \\ 0 & \kappa_1(\gamma_F,\beta_1) \\ 0 & \mathrm{c}\theta_1 \\ 0 & \mathrm{s}\theta_1 \end{bmatrix}\begin{bmatrix}\zeta_F\\ v_1\end{bmatrix}$$

with configuration $\boldsymbol{q} \triangleq [\gamma_F \; \beta_1 \; \boldsymbol{q}_1^\top]^\top$ and input $\boldsymbol{u} = [\zeta_F \; v_1]^\top$.

Remark 8: The derived model (30) is well defined if the curvature $|\kappa_1(\gamma_F,\beta_1)|$ is bounded, which corresponds (see (20)) to the condition $|\delta_1(\gamma_F,\beta_1)| < \pi/2$. Recalling (17), the latter inequality leads to the worst-case condition

$$|\beta_1| < \frac{\pi}{2} - \arctan\left(\frac{L_{h1}}{L_0}\tan\bar\gamma_F\right). \tag{31}$$

Knowing the values of the kinematic parameters of a bus, one can check if (31) is limiting in practice or not. For example, taking the parameters of the *Urbino 18 Electric* articulated bus, manufactured by the Solaris Bus & Coach S.A. company, [4], [27], we have $\bar\gamma_F \approx 42\,\mathrm{deg}$, $\bar\beta_1 \approx 54\,\mathrm{deg}$, $L_{h1} \approx 1.789\,\mathrm{m}$, and $L_0 = 5.9\,\mathrm{m}$. In this case, the inequality (31) leads to $|\beta_1| < b_1 = 74.7\,\mathrm{deg}$. Since $b_1 > \bar\beta_1$, the condition (31) is always satisfied for the *Urbino 18 Electric* bus if only the mechanical limitations imposed by $\bar\beta_1$ are not violated (see Remark 4).

To show modularity of the proposed algorithm, let us select the tractor as a distinguished segment now. In this case, **Step 1** and **Step 2** follow in the same manner as above, thus we need to proceed from the next step.

Step S3: If the tractor is a distinguished segment we take $j = 0$, and now

$$\dot{\boldsymbol{q}}_0 = \boldsymbol{G}(\theta_0,0)\boldsymbol{u}_0, \qquad \boldsymbol{q}_0 = [\theta_0 \; x_0 \; y_0]^\top, \tag{32}$$

since $\gamma_0 \equiv 0$ (by assumption A5).

Step S4: For the *pushing* articulated bus we select $k = 1$. Because $\boldsymbol{u}_1 = [\omega_1 \; v_1]^\top$ is not present in the formula (32), we apply the transformation (14) to write

$$\boldsymbol{u}_0 \overset{(14)}{=} \boldsymbol{J}_1^{-1}(\beta_1,0,0)\boldsymbol{u}_1, \tag{33}$$

where the form of matrix $\boldsymbol{J}_1^{-1}(\beta_1,0,0)$ comes from (26).

Step S5: We express $\boldsymbol{u}_1$ analogously as in (28) using the curvature (29).

Step S6: By collecting the formulas (24), (25), together with (32) and (33), and by replacing $\boldsymbol{u}_1$ with (28), one obtains the following kinematic model (the zero arguments of matrices have been omitted for compactness)

$$\underbrace{\begin{bmatrix} \dot\gamma_F \\ \dot\beta_1 \\ \dot{\boldsymbol{q}}_0 \end{bmatrix}}_{\dot{\boldsymbol{q}}} = \underbrace{\begin{bmatrix} 1 & 0 \\ 0 & \boldsymbol{c}^\top\boldsymbol{\Gamma}_1(\beta_1)\boldsymbol{J}_1^{-1}(\beta_1)\begin{bmatrix}\kappa_1(\gamma_F,\beta_1)\\1\end{bmatrix} \\ \boldsymbol{0} & \boldsymbol{G}(\theta_0)\boldsymbol{J}_1^{-1}(\beta_1)\begin{bmatrix}\kappa_1(\gamma_F,\beta_1)\\1\end{bmatrix} \end{bmatrix}}_{\boldsymbol{S}(\boldsymbol{q})\in\mathbb{R}^{5\times 2}} \underbrace{\begin{bmatrix}\zeta_F\\ v_1\end{bmatrix}}_{\boldsymbol{u}} \tag{34}$$

$$= \begin{bmatrix} 1 & 0 \\ 0 & -\left(1+\frac{L_1}{L_{h1}}\mathrm{c}\beta_1\right)\kappa_1(\gamma_F,\beta_1)+\frac{1}{L_{h1}}\mathrm{s}\beta_1 \\ 0 & (\mathrm{s}\beta_1 - L_1\mathrm{c}\beta_1\kappa_1(\gamma_F,\beta_1))/L_{h1} \\ 0 & (\mathrm{c}\beta_1 + L_1\mathrm{s}\beta_1\kappa_1(\gamma_F,\beta_1))\mathrm{c}\theta_0 \\ 0 & (\mathrm{c}\beta_1 + L_1\mathrm{s}\beta_1\kappa_1(\gamma_F,\beta_1))\mathrm{s}\theta_0 \end{bmatrix}\begin{bmatrix}\zeta_F\\ v_1\end{bmatrix}$$

with configuration $\boldsymbol{q} \triangleq [\gamma_F \; \beta_1 \; \boldsymbol{q}_0^\top]^\top$ and input $\boldsymbol{u} = [\zeta_F \; v_1]^\top$.

2) Modelling a pulling bus with a steerable wagon wheel: Let us go through the particular design steps.

Step S1: Since $\mathcal{I}_s = \{1\}$, we write

$$\dot\gamma_F = \zeta_F \quad \text{and} \quad \dot\gamma_1 = \zeta_1. \tag{35}$$

Step S2: For $i = 1 = N$ we have

$$\dot\beta_1 = \boldsymbol{c}^\top\boldsymbol{\Gamma}_1(\beta_1,\gamma_1,0)\boldsymbol{J}_1^{-1}(\beta_1,\gamma_1,0)\boldsymbol{u}_1, \tag{36}$$

where

$$\boldsymbol{J}_1^{-1}(\beta_1,\gamma_1,0) = \begin{bmatrix} -\frac{L_1}{L_{h1}}\mathrm{c}\beta_1 & \frac{1}{L_{h1}}\mathrm{s}(\beta_1-\gamma_1) \\ L_1\mathrm{s}\beta_1 & \mathrm{c}(\beta_1-\gamma_1) \end{bmatrix} \tag{37}$$

is the inverse transformation matrix (15) in a reduced form obtained for $\gamma_0 \equiv 0$ (by assumption A5).

Step S3: If the wagon is a distinguished segment we take $j = 1$ and

$$\dot{\boldsymbol{q}}_1 \overset{(22)}{=} \boldsymbol{G}(\theta_1,\gamma_1)\boldsymbol{u}_1, \qquad \boldsymbol{q}_1 = [\theta_1 \; x_1 \; y_1]^\top. \tag{38}$$

Step S4: For the *pulling* articulated bus we have to select $k = 0$, determining v_0 as a longitudinal-velocity input of a model. Since $\boldsymbol{u}_0 = [\omega_0 \; v_0]^\top$ is not present in the formulas derived in steps S2-S3, we have to apply the transformation (14) by writing

$$\boldsymbol{u}_1 \overset{(14)}{=} \boldsymbol{J}_1(\beta_1,\gamma_1,0)\boldsymbol{u}_0, \tag{39}$$

where the form of matrix $\boldsymbol{J}_1(\beta_1,\gamma_1,0)$ comes from (14) written for $\gamma_0 \equiv 0$.

Step S5: We express now

$$\boldsymbol{u}_0 = \begin{bmatrix} \kappa_0(\gamma_F) \\ 1 \end{bmatrix} v_0, \tag{40}$$

with the tractor segment curvature $\kappa_0(\gamma_F)$ determined by (19).

Step S6: By collecting the formulas (35), (36), together with (38) and (39), and by replacing $\boldsymbol{u}_0$ with (40), one obtains the

following kinematic model (the zero arguments of matrices have been omitted for compactness)

$$\underbrace{\begin{bmatrix}\dot\gamma_F\\ \dot\beta_1\\ \dot\gamma_1\\ \dot{\boldsymbol{q}}_1\end{bmatrix}}_{\dot{\boldsymbol{q}}} = \underbrace{\begin{bmatrix}1&0&0\\0&0&\boldsymbol{c}^\top\boldsymbol{\Gamma}_1(\beta_1,\gamma_1)\begin{bmatrix}\kappa_0(\gamma_F)\\1\end{bmatrix}\\0&1&0\\\boldsymbol{0}&\boldsymbol{0}&\boldsymbol{G}(\theta_1,\gamma_1)\boldsymbol{J}_1(\beta_1,\gamma_1)\begin{bmatrix}\kappa_0(\gamma_F)\\1\end{bmatrix}\end{bmatrix}}_{\boldsymbol{S}(\boldsymbol{q})\in\mathbb{R}^{6\times3}}\underbrace{\begin{bmatrix}\zeta_F\\\zeta_1\\v_0\end{bmatrix}}_{\boldsymbol{u}} \tag{41}$$

$$= \begin{bmatrix}1&0&0\\0&0&\left(1+\frac{L_{h1}\mathrm{c}(\beta_1-\gamma_1)}{L_1\mathrm{c}\gamma_1}\right)\kappa_0(\gamma_F)-\frac{\mathrm{s}(\beta_1-\gamma_1)}{L_1\mathrm{c}\gamma_1}\\0&1&0\\0&0&(\mathrm{s}(\beta_1-\gamma_1)-L_{h1}\mathrm{c}(\beta_1-\gamma_1)\kappa_0(\gamma_F))\frac{1}{L_1\mathrm{c}\gamma_1}\\0&0&(\mathrm{c}(\theta_1+\gamma_1)\mathrm{c}\beta_1+L_{h1}\mathrm{s}\beta_1\mathrm{c}(\theta_1+\gamma_1)\kappa_0(\gamma_F))\frac{1}{\mathrm{c}\gamma_1}\\0&0&(\mathrm{s}(\theta_1+\gamma_1)\mathrm{c}\beta_1+L_{h1}\mathrm{s}\beta_1\mathrm{s}(\theta_1+\gamma_1)\kappa_0(\gamma_F))\frac{1}{\mathrm{c}\gamma_1}\end{bmatrix}\begin{bmatrix}\zeta_F\\\zeta_1\\v_0\end{bmatrix}$$

with configuration $\boldsymbol{q} \triangleq [\gamma_F \;\; \beta_1 \;\; \gamma_1 \;\; \boldsymbol{q}_1^\top]^\top$ and input $\boldsymbol{u} = [\zeta_F \;\; \zeta_1 \;\; v_0]^\top$.

To illustrate modularity of the proposed approach, let us select the tractor as a distinguished segment. In this case, **Step 1** and **Step 2** follow in the same manner as above, thus we proceed from the next step.

Step S3: If the tractor is a distinguished segment we take $j = 0$, and

$$\dot{\boldsymbol{q}}_0 = \boldsymbol{G}(\theta_0, 0)\boldsymbol{u}_0, \qquad \boldsymbol{q}_0 = [\theta_0 \;\; x_0 \;\; y_0]^\top, \tag{42}$$

since $\gamma_0 \equiv 0$ (by assumption A5).

Step S4: For the *pulling* articulated bus we select $k = 0$. Because $\boldsymbol{u}_0 = [\omega_0 \;\; v_0]^\top$ is not present in the formula (36), we apply the transformation (14) to write the relation (39).

Step S5: We express $\boldsymbol{u}_0$ analogously as in (40) using (19).

Step S6: By collecting the formulas (35), (36), together with (42) and (39), and by replacing $\boldsymbol{u}_0$ with (40), one obtains the following kinematic model (the zero arguments of matrices have been omitted for compactness)

$$\underbrace{\begin{bmatrix}\dot\gamma_F\\ \dot\beta_1\\ \dot\gamma_1\\ \dot{\boldsymbol{q}}_0\end{bmatrix}}_{\dot{\boldsymbol{q}}} = \underbrace{\begin{bmatrix}1&0&0\\0&0&\boldsymbol{c}^\top\boldsymbol{\Gamma}_1(\beta_1,\gamma_1)\begin{bmatrix}\kappa_0(\gamma_F)\\1\end{bmatrix}\\0&1&0\\\boldsymbol{0}&\boldsymbol{0}&\boldsymbol{G}(\theta_0)\begin{bmatrix}\kappa_0(\gamma_F)\\1\end{bmatrix}\end{bmatrix}}_{\boldsymbol{S}(\boldsymbol{q})\in\mathbb{R}^{6\times3}}\underbrace{\begin{bmatrix}\zeta_F\\\zeta_1\\v_0\end{bmatrix}}_{\boldsymbol{u}} \tag{43}$$

$$= \begin{bmatrix}1&0&0\\0&0&\left(1+\frac{L_{h1}\mathrm{c}(\beta_1-\gamma_1)}{L_1\mathrm{c}\gamma_1}\right)\kappa_0(\gamma_F)-\frac{\mathrm{s}(\beta_1-\gamma_1)}{L_1\mathrm{c}\gamma_1}\\0&1&0\\0&0&\kappa_0(\gamma_F)\\0&0&\mathrm{c}\theta_0\\0&0&\mathrm{s}\theta_0\end{bmatrix}\begin{bmatrix}\zeta_F\\\zeta_1\\v_0\end{bmatrix}$$

with configuration $\boldsymbol{q} \triangleq [\gamma_F \;\; \beta_1 \;\; \gamma_1 \;\; \boldsymbol{q}_0^\top]^\top$ and input $\boldsymbol{u} = [\zeta_F \;\; \zeta_1 \;\; v_0]^\top$.

B. Derivation of a model for a bus with a double articulation

Figure 5 illustrates a kinematic structure of a three-body bi-articulated bus ($N = 2$). In this structure, the first wagon's axle is driven ($k = 1$) but is non-steerable, while the second wagon's axle is non-driven but steerable ($\mathcal{I}_s = \{2\}$) – it is practically justified due to a considerable length of the vehicle. We can call this kind of a vehicle the *pushing-pulling* bus (or *pusher-puller*), see [4]. Let us go through the particular design steps.

Step S1: Since $\mathcal{I}_s = \{2\}$, we write

$$\dot\gamma_F = \zeta_F \quad \text{and} \quad \dot\gamma_2 = \zeta_2. \tag{44}$$

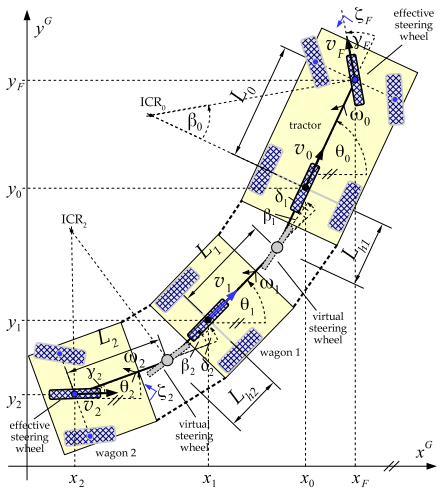

Figure 5. A kinematic structure of a bi-articulated *pushing-pulling* bus with a driven but non-steerable first wagon axle and a non-driven but steerable second wagon axle; kinematic control inputs are highlighted in blue.

Step S2: For $i = 1$ and $i = 2$ we have

$$\dot\beta_1 = \boldsymbol{c}^\top\boldsymbol{\Gamma}_1(\beta_1, 0, 0)\boldsymbol{J}_1^{-1}(\beta_1, 0, 0)\boldsymbol{u}_1, \tag{45}$$

$$\dot\beta_2 = \boldsymbol{c}^\top\boldsymbol{\Gamma}_2(\beta_2, \gamma_2, 0)\boldsymbol{J}_2^{-1}(\beta_2, \gamma_2, 0)\boldsymbol{u}_2, \tag{46}$$

where $\boldsymbol{J}_1^{-1}(\beta_1, 0, 0)$ results from (26), while

$$\boldsymbol{J}_2^{-1}(\beta_2, \gamma_2, 0) = \begin{bmatrix}-\frac{L_2}{L_{h2}}\mathrm{c}\beta_2 & \frac{1}{L_{h2}}\mathrm{s}(\beta_2-\gamma_2)\\ L_2\mathrm{s}\beta_2 & \mathrm{c}(\beta_2-\gamma_2)\end{bmatrix} \tag{47}$$

is the inverse transformation matrix (15) in a reduced form obtained for $\gamma_1 \equiv 0$.

Step S3: If the second wagon is a distinguished segment we take $j = 2$ and

$$\dot{\boldsymbol{q}}_2 \overset{(22)}{=} \boldsymbol{G}(\theta_2, \gamma_2)\boldsymbol{u}_2, \qquad \boldsymbol{q}_2 = [\theta_2 \;\; x_2 \;\; y_2]^\top. \tag{48}$$

Step S4: For the *pushing-pulling* bi-articulated bus we select $k = 1$, determining v_1 as a longitudinal-velocity input of a model. Since $\boldsymbol{u}_1 = [\omega_1 \;\; v_1]^\top$ is not present in the formulas (46) and (48), we have to apply the transformation (14) to write

$$\boldsymbol{u}_2 \overset{(14)}{=} \boldsymbol{J}_2(\beta_2, \gamma_2, 0)\boldsymbol{u}_1, \tag{49}$$

where the form of matrix $\boldsymbol{J}_2(\beta_2, \gamma_2, 0)$ comes from (14) written for $\gamma_1 \equiv 0$.

Step S5: We express $\boldsymbol{u}_1$ analogously as in (28) using the curvature (29).

Step S6: By collecting the formulas (44), (45)-(46), together with (48) and (49), and by replacing $\boldsymbol{u}_1$ with (28), one obtains the following kinematic model (the zero arguments of matrices have been omitted for compactness)

$$\underbrace{\begin{bmatrix}\dot\gamma_F\\ \dot\beta_1\\ \dot\beta_2\\ \dot\gamma_2\\ \dot{\boldsymbol{q}}_2\end{bmatrix}}_{\dot{\boldsymbol{q}}} = \underbrace{\begin{bmatrix}1&0&0\\0&0&\boldsymbol{c}^\top\boldsymbol{\Gamma}_1(\beta_1)\boldsymbol{J}_1^{-1}(\beta_1)\begin{bmatrix}\kappa_1(\gamma_F,\beta_1)\\1\end{bmatrix}\\0&0&\boldsymbol{c}^\top\boldsymbol{\Gamma}_2(\beta_2,\gamma_2)\begin{bmatrix}\kappa_1(\gamma_F,\beta_1)\\1\end{bmatrix}\\0&1&0\\\boldsymbol{0}&\boldsymbol{0}&\boldsymbol{G}(\theta_2,\gamma_2)\boldsymbol{J}_2(\beta_2,\gamma_2)\begin{bmatrix}\kappa_1(\gamma_F,\beta_1)\\1\end{bmatrix}\end{bmatrix}}_{\boldsymbol{S}(\boldsymbol{q})\in\mathbb{R}^{7\times3}}\underbrace{\begin{bmatrix}\zeta_F\\\zeta_2\\v_1\end{bmatrix}}_{\boldsymbol{u}} \tag{50}$$

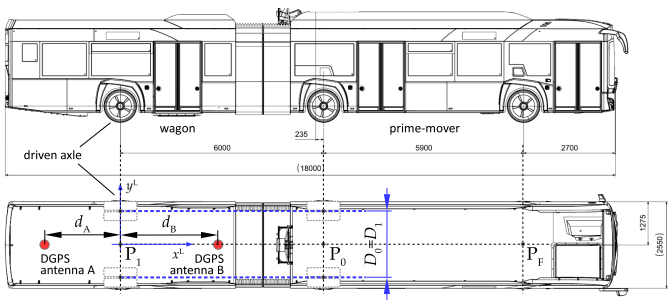

Figure 6. Drawings of the *Urbino 18 Electric* pushing articulated urban bus used in the validation experiments; the locations of two DGPS antennas mounted on the wagon's roof are denoted.

with configuration $\boldsymbol{q} \triangleq [\gamma_F \ \beta_1 \ \beta_2 \ \gamma_2 \ \boldsymbol{q}_2^\top]^\top$ and input $\boldsymbol{u} = [\zeta_F \ \zeta_2 \ v_1]^\top$.

Remark 9: It is worth stressing that the proposed methodology can be also applied to modelling the tractor-trailer (more general: N-trailer) vehicles, [1], [9]. For example, if we consider the *pulling* bi-articulated bus ($N = 2$), [6], where the rear axle of a tractor is driven ($k = 0$) and if axles of both wagons are steerable ($\mathcal{I}_s = \{1, 2\}$), then application of the modelling algorithm, and treating the last wagon as a distinguished segment, leads to the kinematics (cf. [34])

$$\underbrace{\begin{bmatrix} \dot\gamma_F \\ \dot\beta_1 \\ \dot\beta_2 \\ \dot\gamma_1 \\ \dot\gamma_2 \\ \dot{\boldsymbol{q}}_2 \end{bmatrix}}_{\dot{\boldsymbol{q}}} = \underbrace{\begin{bmatrix} 1 & 0 & 0 & 0 \\ 0 & 0 & 0 & \boldsymbol{c}^\top \boldsymbol{\Gamma}_1(\beta_1,\gamma_1)\begin{bmatrix}\kappa_0(\gamma_F)\\ 1\end{bmatrix} \\ 0 & 0 & 0 & \boldsymbol{c}^\top \boldsymbol{\Gamma}_2(\beta_2,\gamma_2,\gamma_1)\boldsymbol{J}_1(\beta_1,\gamma_1)\begin{bmatrix}\kappa_0(\gamma_F)\\ 1\end{bmatrix} \\ 0 & 1 & 0 & 0 \\ 0 & 0 & 1 & 0 \\ \boldsymbol{0} & \boldsymbol{0} & \boldsymbol{0} & \boldsymbol{G}(\theta_2,\gamma_2)\boldsymbol{J}_2(\beta_2,\gamma_2,\gamma_1)\boldsymbol{J}_1(\beta_1,\gamma_1)\begin{bmatrix}\kappa_0(\gamma_F)\\ 1\end{bmatrix} \end{bmatrix}}_{\boldsymbol{S}(\boldsymbol{q}) \in \mathbb{R}^{8\times 4}} \underbrace{\begin{bmatrix} \zeta_F \\ \zeta_1 \\ \zeta_2 \\ v_0 \end{bmatrix}}_{\boldsymbol{u}}$$

where the steering angles γ_1 and γ_2 belong to the eight-dimensional configuration vector, whereas a control input is four-dimensional now. The above model is equivalent to the multi-steering 2-trailer kinematics [43], [37] (more strictly: multi-steering non-Standard 2-Trailer kinematics, [9]). Since in the case of N-trailers the driving axle is usually placed on a tractor segment ($k = 0$), any inverse transformation matrices (15) are not required in a formulation of the kinematic model. As a consequence, the proposed modular modelling concept can be directly applied to the N-trailer vehicles with any type of hitching (i.e., admitting $L_{hi} > 0$, $L_{hi} < 0$, and also the on-axle interconnections for which $L_{hi} = 0$).

V. Exemplary Experimental Validation

The model of a pushing articulated bus, represented by formula (30), has been experimentally validated using the *Urbino 18 Electric* vehicle (manufactured by the Solaris Bus&Coach S.A. company[1]) presented with dimensions in Fig. 6 (cf. Fig. 1). The kinematic parameters of the bus are collected in Table I. During the experimental tests, the following signals were available on board: the angles of a steering wheel α_{sensor} and of a vehicle's joint $\beta_{1\text{sensor}}$ provided by the build-in sensors, the longitudinal velocity $v_{0\text{tacho}}$ of a fixed-axle's mid-point $P_0 = (x_0, y_0)$ of a tractor provided by a tachometer,

[1]https://www.solarisbus.com/en

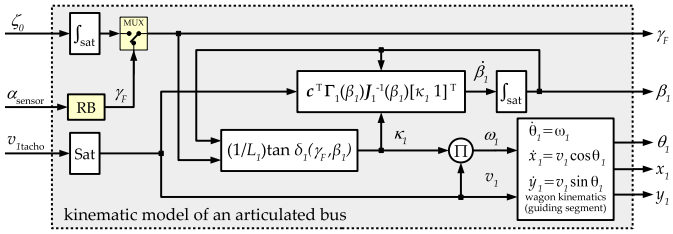

Figure 7. An implementation scheme of the simulation model (30) used for the validation purposes (RB = reconstruction block).

the angular speeds $\mu_{R\text{encoder}}$ (right) and $\mu_{L\text{encoder}}$ (left) of the wagon's wheels, as well as $\nu_{R\text{encoder}}$ (right) and $\nu_{L\text{encoder}}$ (left) of the fixed tractor's wheels, estimated upon the measurements obtained from the wheels' encoders, and global coordinates (x_j, y_j), $j \in \{A, B\}$, of two DGPS antennas mounted on a wagon's roof as depicted in Fig. 6. The signals were recorded with a sampling interval $T_p = 1\,\text{s}$ for the DGPS source, and a mean sampling interval $T_d \approx 0.005\,\text{s}$ for all other sources. Upon the available measurements, the following *ground-truth* signals have been reproduced off-line for the model validation purposes: the steering angle γ_F of an effective steering wheel of a tractor (cf. Fig. 4) reconstructed upon α_{sensor} and a steering mechanism characteristic (see Appendix A), DGPS-based coordinates of the point $P_1 := (x_{1\text{DGPS}}, y_{1\text{DGPS}})$ and the orientation $\theta_{1\text{DGPS}}$ of a wagon's body in a global frame, the longitudinal speed $v_{1\text{tacho}}$ of point P_1, and the pairs of angular velocities $\omega_{0\text{tacho}}$, $\omega_{0\text{encoder}}$ and $\omega_{1\text{tacho}}$, $\omega_{1\text{encoder}}$ of the tractor's and wagon's bodies, respectively. The velocities have been computed according to the formulas:

$$\begin{aligned} \omega_{0\text{tacho}} &:= (v_{0\text{tacho}} \tan\gamma_F)/L_0, \\ \omega_{0\text{encoder}} &:= r_e(\nu_{R\text{encoder}} - \nu_{L\text{encoder}})/D_0, \\ \begin{bmatrix}\omega_{1\text{tacho}} \\ v_{1\text{tacho}}\end{bmatrix} &:= \boldsymbol{J}_1(\beta_{1\text{sensor}}, 0, 0)\begin{bmatrix}\omega_{0\text{tacho}} \\ v_{0\text{tacho}}\end{bmatrix}, \\ \omega_{1\text{encoder}} &:= r_e(\mu_{R\text{encoder}} - \mu_{L\text{encoder}})/D_1, \end{aligned} \tag{51}$$

where r_e denotes an *effective dynamic radius* of a bus wheel (for derivations and details see, e.g., [23], pp. 249-250, or [39]), while D_0 and D_1 represent the spacings of the tractor's and wagon's wheels, respectively (see Table I and Fig. 6).

An implementation scheme of the simulation model (30) used for the validation purposes is presented in Fig. 7. Note that in practical conditions, the bus is equipped with a steering

Table I
Selected kinematic parameters of the experimental bus

parameter	value	description
r_e	0.467 m	effective radius of a wheel
L_0	5.900 m	tractor's length
L_{h1}	1.789 m	hitching offset
L_1	4.211 m	wagon's length
D_F	2.104 m	spacing of tractor's steering wheels
D_0	1.862 m	spacing of tractor's fixed wheels (cf. Fig. 6)
D_1	1.862 m	spacing of wagon's wheels (cf. Fig. 6)
d_A	2.557 m	distance from P_1 to antenna A
d_B	3.268 m	distance from P_1 to antenna B
$\bar\beta_1$	54 deg	maximal admissible absolute joint angle

angle sensor of a steering-wheel instead of a steering rate sensor. Therefore, the block scheme in Fig. 7 contains the MUX block which switches the source of angle γ_F from an output of the integrator directly to an output of the steering-angle reconstruction block (RB, see Appendix A). As a consequence, the two inputs to the model are now: the reconstructed steering angle γ_F and the longitudinal wagon's velocity $v_{1\text{tacho}}$.

Validation experiments have been conducted for three scenarios: for a slanted parking maneuver (Sc1), for a loop-ride maneuver (Sc2), and for a bus-bay transit menauver (Sc3). In scenario Sc1, a human driver brought the vehicle from an initial stop configuration to a final stop configuration inside a slantwise located parking lot. In scenario Sc2, a driver moved the bus along a loop-path in the counterclockwise direction. During the Sc3 scenario, a driver entered with the vehicle a bus bay, stopped the vehicle for a while, and next departed the bus bay. The model inputs, $\gamma_F(t)$ and $v_{1\text{tacho}}(t)$, recorded for all three motion scenarios are provided in Fig. 8. For all the scenarios, the validated model outputs were initialized with the first measurement data points, that is, $\boldsymbol{q}(0) := [\gamma_F(0)\ \beta_{1\text{sensor}}(0)\ \theta_{1\text{DGPS}}(0)\ x_{1\text{DGPS}}(0)\ y_{1\text{DGPS}}(0)]^\top$. Selected validation results obtained for the scenarios Sc1, Sc2, and Sc3 are illustrated in Figs. 9, 10, and 11, respectively.

Effectiveness of the model can be assessed by analysing the differences between the ground-truth plots vs. the corresponding model responses obtained upon:

- **the integral-based** computations – by comparing the pairs of paths $(x_{1\text{DGPS}}, y_{1\text{DGPS}})$ vs. $(x_{1\text{model}}, y_{1\text{model}})$, and the plots $\theta_{1\text{DGPS}}(t)$ vs. $\theta_{1\text{model}}(t)$, and $\beta_{1\text{sensor}}(t)$ vs. $\beta_{1\text{model}}(t)$,
- **the non-integral-based** computations – by comparing the plots of the angular speeds $\omega_{1\text{encoder}}(t)$ vs. $\omega_{1\text{tacho}}(t)$ vs. $\omega_{1\text{model}}(t)$, and the joint-angle rates $\dot{\beta}_{1\text{encoder}}(t) := \omega_{0\text{encoder}}(t) - \omega_{1\text{encoder}}(t)$ vs. $\dot{\beta}_{1\text{tacho}}(t) := \omega_{0\text{tacho}}(t) - \omega_{1\text{tacho}}(t)$ vs. $\dot{\beta}_{1\text{model}}(t)$.

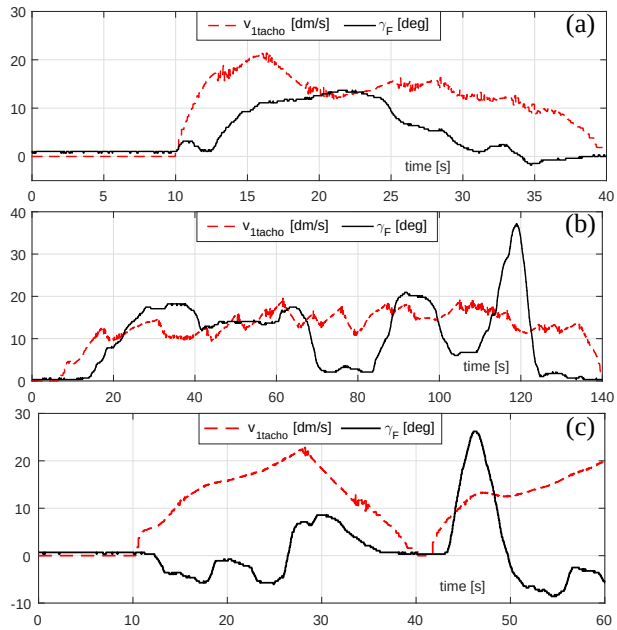

Figure 8. Input signals applied to the simulation model of an articulated bus for the validation purposes: (a) for the parking scenario Sc1, (b) for the loop-ride scenario Sc2, and (c) for the bus-bay transit scenario Sc3; for clarity, $v_{1\text{tacho}}$ is expressed in decimeters per second.

Upon the plots provided in Figs. 9-11, one may observe an acceptable match of the model speeds $\omega_{1\text{model}}(t)$ and $\dot{\beta}_{1\text{model}}(t)$ with those obtained from the encoders, that is, $\omega_{1\text{encoder}}(t)$ and $\dot{\beta}_{1\text{encoder}}(t)$. Larger discrepancies can be seen relative to the velocities $\omega_{1\text{tacho}}(t)$ and $\dot{\beta}_{1\text{tacho}}(t)$, but mostly within the time intervals corresponding to larger differences $|\beta_{1\text{sensor}}(t) - \beta_{1\text{model}}(t)|$ (see the way of computation for $\omega_{1\text{tacho}}$ in (51)). The latter differences seem to be caused by the backlash-like effects, observed in the evolution of signal $\beta_{1\text{sensor}}(t)$, which have not been taken into account in the validated model (30). The initial measurement offset visible in the response of $\beta_{1\text{sensor}}$ in the scenario Sc1 (see Fig. 9) is probably also a result of the backlash in the joint-angle sensor mounting (a small jump of $\beta_{1\text{sensor}}$ on the value of about $2.5\,\text{deg}$ occurred after the first two samples of the measurement). The offset has been naturally deleted when a physical joint angle $\beta_1(t)$ reached and exceeded the offset value during the maneuver. Similar effects are visible also in the plots of $\beta_{1\text{sensor}}(t)$ during the vehicle motion between the 40th and 60th second in the scenario Sc2 (see Fig. 10) and between the 20th and 25th second in the scenario Sc3 (see Fig. 11).

The response mismatches obtained for the integral-based computations (visible when comparing $\theta_{1\text{DGPS}}(t)$ vs. $\theta_{1\text{model}}(t)$, $\beta_{1\text{sensor}}(t)$ vs. $\beta_{1\text{model}}(t)$, and looking at the paths drawn by the vehicle and by the model) are caused by the well-known inherent fragility of these kind of computations on the (unavoidable) integration-error accumulation (drift) which, in general, may boundlessly increase in time. All the uncertainties of the kinematic parameters from Table I and non-modelled effects (like the mechanical backlash effects, temporary skid/slip phenomena of the wheels, the *jitter effect* and limited sampling frequency of measured signals, etc.) can cause an accumulation of the response mismatch between the simulating model and the real system due to a process of the model integration, see [31], [41]. The drift error is especially visible in the plot of $\theta_{1\text{model}}(t)$ for the scenario Sc3. In this case (in contrast to scenarios Sc1 and Sc2), the wagon's motion curvature changed its sign during the maneuver (see the negative and positive signs of the angular velocities $\omega_{1\text{model}}$ and $\omega_{1\text{tacho}}$ in Fig. 11); we suppose that in these conditions the backlash effects of the joint angle sensor and of the steering mechanism caused an additional accumulation of the integration errors in the wagon's orientation variable (cf. Fig. 7 to verify that $\omega_1 := \kappa_1(\gamma_F, \beta_1)v_1$ in the implemented model, and note that $\theta_1(t) = \theta_1(0) + \int_0^t \omega_1(\tau)\mathrm{d}\tau$). As a consequence, the integral-based responses of the model can be reliably utilized only for a short-distance (short-time) quality assessment. Alternatively, one can use a *prediction model* (instead of the simulation model). A prediction model has been implemented for the scenario Sc3 to show a possible improvement of the model's accuracy by utilizing the selected measurements available on a vehicle board. To this aim the angular velocity $\omega_1(t)$ in the implementation scheme from Fig. 7 has been replaced directly with the $\omega_{1\text{tacho}}(t)$ signal

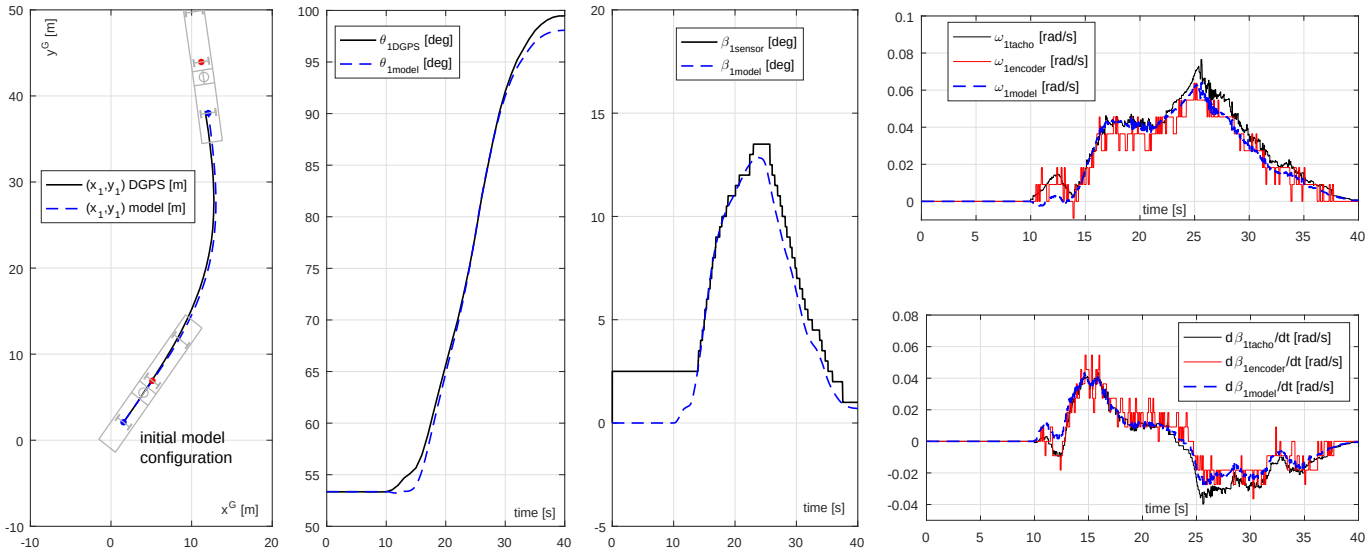

Figure 9. Sc1: Validation results for the simulation model of an articulated vehicle in the case of a parking maneuver obtained with the *Urbino 18 Electric* urban bus.

computed according to (51). The improved results obtained in this case (for both the orientation angle and the positional path) are illustrated by the magenta dash-dot plots in Fig. 11 (labelled as the *prediction-model*).

In contrast to the mentioned drifting problems, the response mismatches obtained for the non-integral-based computations of the model (see the plots of $\dot{\beta}_{1\text{model}}$ and $\omega_{1\text{model}}$) are free of the numerical-integration drift and can be used for a reliable long-distance (long-time) model evaluation.

VI. Relating the Kinematic and Kinetic Modelling Approaches

The nonlinear kinematic modelling approach has been formulated upon the *first principles* of the geometry of velocities. The essential approximations characterizing the method come from the simplifying assumptions A1-A6 formulated in

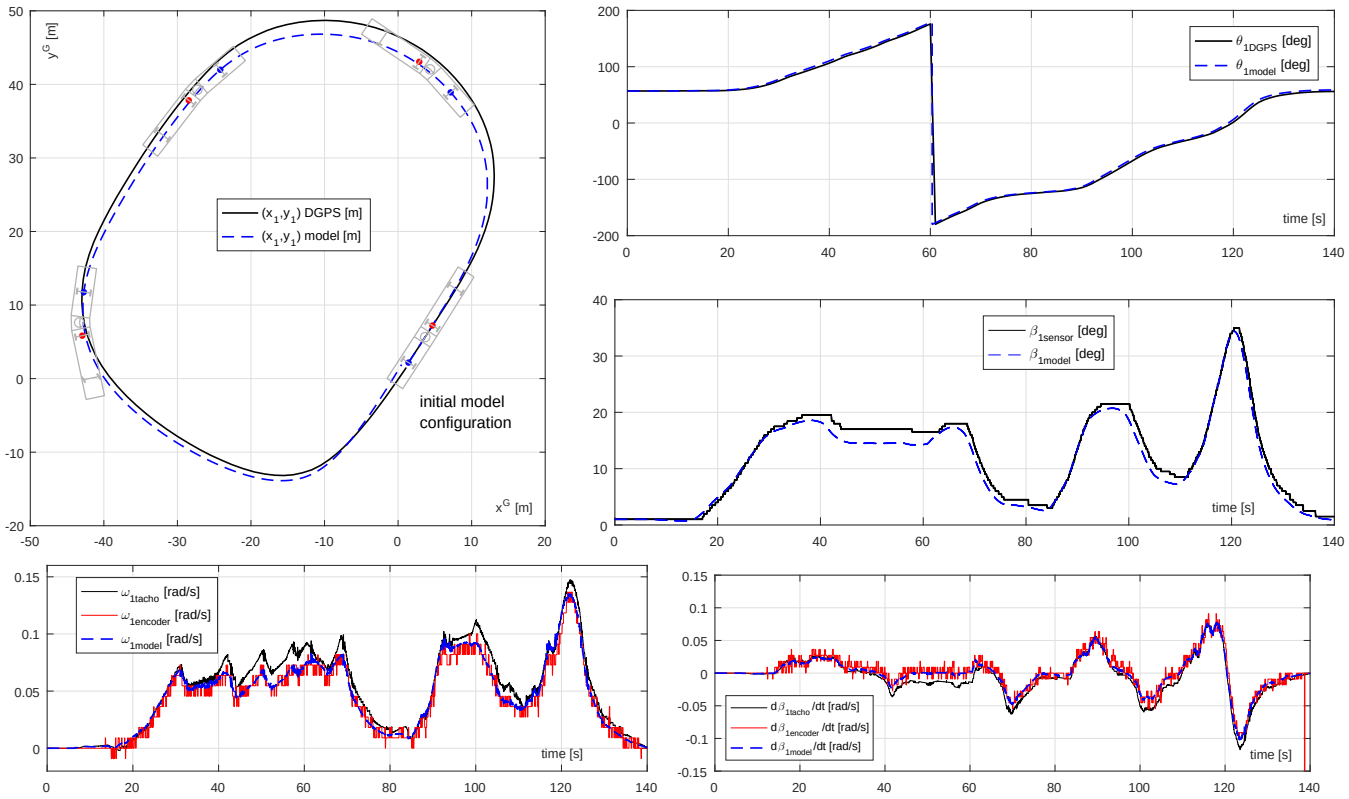

Figure 10. Sc2: Validation results for the simulation model of an articulated vehicle in the case of a loop-ride maneuver obtained with the *Urbino 18 Electric* urban bus.

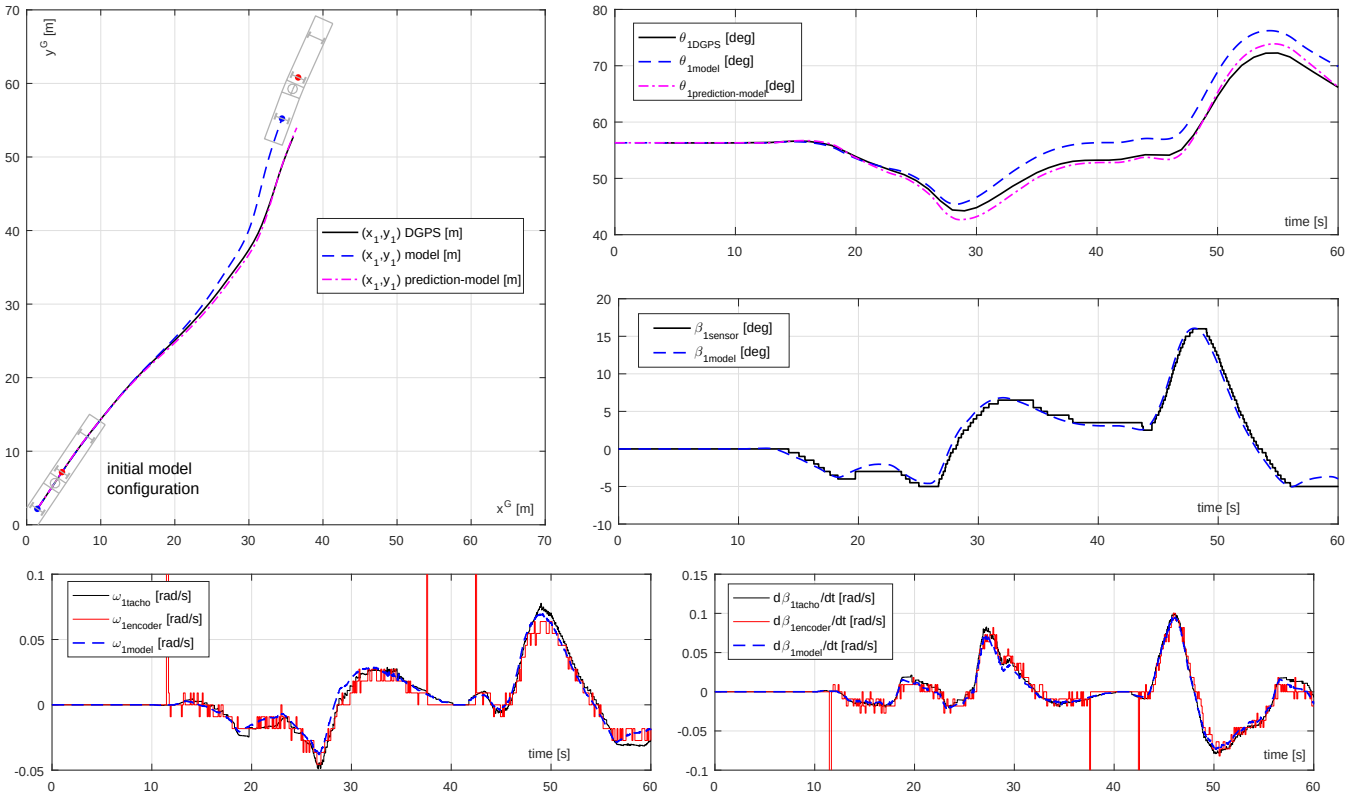

Figure 11. Sc3: Validation results for the articulated bus model in the case of a bus-bay transit maneuver obtained with the *Urbino 18 Electric* urban bus (the results denoted by the dash-dot magenta plots represent a response of the *prediction-model*, i.e., the model with $\omega_1(t) := \omega_{1\text{tacho}}(t)$ instead of $\omega_{1\text{model}}(t)$); the three sets of outliers visible on the plot of angular velocity $\omega_{1\text{encoder}}$ (and, consequently, on the plot of $\mathrm{d}\beta_{1\text{encoder}}/\mathrm{d}t$) around 12th, 38th, and 43rd seconds result from occasional perturbations affecting a velocity measurement system of the bus.

Section II-A. As a consequence, one can try to relate the proposed modelling methodology to alternative approaches known from the literature through the validity of assumptions A1-A6. In this context, an underlying alternative is the *kinetic* ('dynamic') approach to modelling of the vehicles, which takes into account the effects of masses, inertias, friction, drag, elasticity, gravity, etc. Let us qualitatively compare the benefits and limitations of the proposed kinematic modelling with properties of the modular kinetic modelling approach recently proposed in [44]. The two methods are comparable in the sense of their application range and a modularity level.

The main comparative conclusions can be formulated upon the table presented in Fig. 12. The most significant benefit of the kinetic models result from their high-fidelity and validity in a wide range of velocities and accelerations. Thanks to this property, the kinetic models can describe and explain those physical effects which are not modelled by the purely kinematic models. This benefit, however, to be practically useful requires the high precision knowledge of the numerous model parameters (hardly measurable, and often time-varying), good approximations of the complex physical phenomena (like the wheels-ground interaction, aerodynamic drag, skid-slip motion of the wheels, etc.), and a limited complexity of a resultant model to be applicable with a usage of reasonable computational resources. From the high-complexity models one shall expect higher sensitivity of their response to the parametric and structural uncertainties, leading to their limited effectiveness in some practical applications. In contrast, the kinematic models have a much simpler structure, with only few kinematic parameters, which are easily and precisely measurable, and usually do not change in time. Therefore, if one is interested mainly in the low-speed smooth motion description, the use of kinematic modelling becomes a good compromise between the fidelity and complexity. The next important difference between the models presented in [44] and those resulting from the proposed kinematic approach comes from a physical nature of their control inputs. The kinetic models are usually driven by the tire forces (or other *generalized forces* defined on an upper level) which, despite their closeness to the physical origins of motion, are very difficult to measure in practice. As a consequence, computations of the kinetic models in parallel to a real vehicle (required by numerous applications of the models) may become very problematic. Whereas the kinematic models accept the velocity-like control inputs, which are easily measurable (or reproducible) by using the conventional sensors available in the contemporary vehicles. A scalability level of the kinetic and kinematic modelling approaches, with respect to a number of wagons/trailers, seems to be different as well. The kinetic models from [44], although scalable, are much more complex. Thus any extension of a kinetic model with additional wagons is non-trivial. Whereas, scalability of the kinematic models proposed in the current paper is very high and can be easily automated. Finally, an engineering utilization of the kinetic models and the kinematic models is motivated by different objectives. The former are often preferable in the high-fidelity training simulators and in the control problems

Proposed modular KINEMATIC modelling		Alternative modular KINETIC ('DYNAMIC') modelling	
Benefits	Limitations	Benefits	Limitations
B1. **Leads to simple-structure models:** - low cost of a model usage in practice (preferable for the embedded applications), - closed form of a non-linear model, - models derived from the first principles (clear physical interpretations), - preferable in the low-speed motion planning and motion control for intelligent and autonomous vehicles. B2. **Velocity-like inputs:** - easily measurable in the real vehicles, - natural for the electrical servo drives, B3. **Low parametric uncertainty:** - relatively small number of parameters, - values of most kinematic parameters are constant and measured with high precision. B4. **High scalability** with respect to a number of wagons/trailers. B5. **Simulation of the model requires only a single integration process** (minor numerical drift).	L1. **Restricted usage** to the low-speed and low-acceleration motion conditions (non-holonomic constraints only approximately satisfied). L2. **Describes only a planar motion of a vehicle** perpendicular to the gravity acce-leration vector (up-hill/down-hill motion, slippery motion, and the roll and pitch degrees of freedom are not addressed). L3. **Does not describe any kinetic effects** like dissipation of energy, inertia of vehicle's bodies, resonances, elasticity of vehicle's bodies, dead-zones, slippage/skidding of the wheels, etc.	B1. **Leads to high-fidelity models:** - applications within a wide range of velo-cities and accelerations of a vehicle, - models derived from the first principles (clear physical interpretations), - describes kinetic and kinematic effects, - wheels slippage and skidding are admitted. B2. **Model inputs usually in the form of generalized forces** – closer to the physical origins of motion of a vehicle. B3. **Preferable in high-fidelity motion simulators and in control applications for the 'dynamical' tasks** like the rollover prevention, yaw stability control, anti-slip braking, dynamic-jackknife prevention, etc.	L1. **Complexity of the models:** - higher cost of a model usage in practice (especially for multi-body vehicles), - fast dynamical modes require fast sampling, - higher sensitivity to model uncertainties, - often approximated by a linear form (only local validity). L2. **Difficulties with control inputs (forces):** - hardly measurable in the real vehicles, - practical control inputs are related to actua-tors which have to be modelled (complexity). L3. **Higher uncertainties possible:** - large number of model parameters, - values of parameters often unknown (hardly measurable) or/and time-varying, - structural errors occur when modelling complex kinetic effects (approximations). L4. **Lower scalability** with respect to a number of wagons/trailers. L5. **Simulation of the model requires a double integration process** (larger numerical drift).

Figure 12. Qualitative comparison of the benefits and limitations characterising the proposed kinematic modelling methodology and the alternative modular kinetic ('dynamic') modelling approach proposed in [44].

related to the 'dynamical' tasks (e.g., the rollover prevention, yaw stabilization, anti-slip braking, etc., [39]). The kinematic models, in turn, are preferable in the problems of real-time motion planning and higher-level control design for the low-speed maneuvering, and in particular for the so-called embedded solutions. Summarizing, both the kinetic and kinematic models of the articulated vehicles have their benefits and limitations. When we treat them as complementary engineering tools, they can be useful to solve different practical problems. A reasonable selection of a model shall be a consequence of a compromise between a usage-price and efficiency.

VII. Concluding remarks

We have proposed the generic framework for modelling kinematics of the (multi-)articulated vehicles with various locus of a driving axle and various steering capabilities. The main benefits of the method come from its scalability (with respect to a number of vehicle's segments), and modularity which allows for a straightforward (even automated) derivation of compact models which are tractable in real-time by relatively low-power computing devices. The latter property is especially important in the context of embedded applications for the intelligent or automated vehicles. The models can be useful, in particular, for purposes of the higher-level control design and model-based control, motion planning, and vehicle localization, mostly in the tasks of low-speed maneuvering in the conditions of sufficient friction forces between the wheels and a ground, where any practical effects caused by a potential micro skid-slip motion can be neglected. The inherent limitations of the kinematic modelling come from the limiting assumptions formulated in Section II-A, for which the models have been derived. As a consequence of violating the assumptions A1-A3, the models may become non-efficient in those applications which require a highly dynamic motion in a rough terrain, or a motion on the slippery and/or sloppy surfaces. Violation of assumptions A5-A6 seems to not happen in the domain of articulated buses, but may concern some other special constructions of vehicles (not covered directly by the proposed modelling approach). The authors are currently using the derived models to motion algorithmization of articulated urban buses with applications to the advanced driver assistance systems (ADAS).

Appendix A

A steering mechanism of the *Urbino 18 Electric* bus is based on the hydraulic RB-Servocom system, with an angular-position sensor mounted in a steering gear or on a steering column. Upon the test measurements, collected by the Homologation and Test Department of the Solaris Bus & Coach Company, [27], we derived a static mapping, $\gamma_F = f_\gamma(\alpha_{\text{sensor}})$, between the steering angle α_{sensor} (measured by the angular-position sensor) and the (virtual) steering angle γ_F of a prime-mover's effective steering wheel, using the well known formulas of the Ackermann steering geometry. The resultant steering mapping $\gamma_F[\text{deg}] = f_\gamma(\alpha_{\text{sensor}}[\text{deg}])$ for the *Urbino 18 Electric* bus was approximated by the following equation (limiting here the coefficients to two significant digits):

$$\gamma_F \approx 3.2 \cdot 10^{-5}\alpha^3_{\text{sensor}} + 9.8 \cdot 10^{-5}\alpha^2_{\text{sensor}} + 0.71\alpha_{\text{sensor}} + 0.69,$$

where the particular coefficients of the above formula were found by using a conventional least squares fitting method.

References

[1] C. Altafini. Some properties of the general n-trailer. *Int. Journal of Control*, 74(4):409–424, 2001.
[2] F. Altche, P. Polack, and A. de La Fortelle. A simple dynamic model for aggressive, near-limits trajectory planning. In *2017 IEEE Intell. Vehicles Symp.*, pages 141–147, Redondo Beach, USA, 2017.
[3] K. Bengler, K. Dietmayer, B. Farber, M. Maurer, C. Stiller, and H. Winner. Three decades of driver assistance systems. Review and future perspectives. *IEEE Intell. Transp. Sys. Mag.*, 6(4):6–22, 2014.
[4] Solaris Bus&Coach. Alternative powertrain. *Product catalogue*, 2018.
[5] W. Chung and K. Iagnemma. Wheeled robots. In B. Siciliano and O. Khatib, editors, *Springer Handbook of Robotics. 2nd Edition*, pages 575–593. Springer, 2016.

[6] H.A. Dang and J. Kovanda. Determination of trajectory of articulated bus turning along curved line. *Trans. Transp. Scien.*, 7(1):35–44, 2014.
[7] D. de Bruin and P.P.J. van den Bosch. Modelling and control of a double articulated vehicle with four steerable axles. In *Proc. American Control Conference (ACC)*, pages 3250–3254, 1999.
[8] X. Ding, S. Mikaric, and Y. He. Design of an active trailer-steering system for multi-trailer articulated heavy vehicles using real-time simulations. *Proc. IMechE PartD: J. Automob. Eng.*, 227(5):643–655, 2013.
[9] M. Michałek. Non-minimum-phase property of N-trailer kinematics resulting from off-axle interconnections. *Int. Journal of Control*, 86(4):740–758, 2013.
[10] T. Gawron, M. Mydlarz, and M.M. Michałek. Algorithmization of constrained monotonic maneuvers for an advanced driver assistant system in the intelligent urban buses. In *2019 IEEE Intelligent Vehicles Symposium (IV)*, pages 218–224, Paris,France, 2019.
[11] V. Girbes, L. Armesto, J. Dols, and J. Tornero. Haptic feedback to assist bus drivers for pedestrian safety at low speed. *IEEE Trans. Haptics*, 9(3):345–357, 2016.
[12] D. Goehlich, T.-A. Fay, D. Jefferies, E. Lauth, A. Kunith, and X. Zhang. Design of urban electric bus systems. *Des. Sci.*, 4(e15):1–28, 2018.
[13] D. Gonzalez, J. Perez, V. Milanes, and F. Nashashibi. A review of motion planning techniques for automated vehicles. *IEEE Trans. Intell. Transp. Sys.*, 17(4):1135–1145, 2016.
[14] F. Gottmann, H. Wind, and O. Sawodny. On the influence of rear axle steering and modeling depth on a model based racing line generation for autonomous racing. In *IEEE CCTA*, pages 846–852, Copenhagen, 2018.
[15] B. Hemily and R.D. King. *Uses of higher capacity of buses in transit service*. Transportation Research Board, Washington D.C., 2008.
[16] J. Huang and H.-S. Tan. Control system design of an automated bus in revenue service. *IEEE Trans. ITS*, 17(10):2868–2878, 2016.
[17] J. Huang and H.-S. Tan. Development and validation of an automated steering control system for bus revenue service. *IEEE Trans. Autom. Sci. Engineering*, 13(1):227–237, 2016.
[18] F. Jean. The car with N trailers: characterisation of the singular configurations. *Control, Opt. Calc. Variations*, 1:241–266, 1996.
[19] B.A. Jujnovich and D. Cebon. Path-following steering control for articulated vehicles. *ASME J. Dynamic Systems, Measurement, and Control*, 135:031006–1–031006–15, 2013.
[20] C. M. Kang, S.-H. Lee, and C. C. Chung. Comparative evaluation of dynamic and kinematic vehicle models. In *53rd IEEE Conf. Decision and Control*, pages 648–653, Los Angeles, USA, 2014.
[21] M. Karkee and B.L. Steward. Study of the open and closed loop characteristics of a tractor and a single axle towed implement system. *J. Terramechanics*, 47:379–393, 2010.
[22] E. Kayacan, E. Kayacan, H. Ramon, and W. Saeys. Learning in centralized nonlinear model predictive control: Application to an autonomous tractor-trailer system. *IEEE TCST*, 23(1):197–205, 2015.
[23] U. Kiencke and L. Nielsen. *Automotive Control Systems. For Engine, Driveline, and Vehicle*. Springer-Verlag, SAE International, Berlin Heidelberg, 2000.
[24] Y.C. Kim, K.-H. Yun, and K.-D. Min. Automatic guidance control of an articulated all-wheel-steered vehicle. *Vehicle System Dynamics*, 52(4):456–474, 2014.
[25] K. Kivekäs, A. Lajunen, F. Baldi, J. Vepsäläinen, and K. Tammi. Reducing the energy consumption of electric buses with design choices and predictive driving. *IEEE TVT*, 68(12):11409 – 11419, 2019.
[26] I. Kowarska, J. Korta, K. Kuczek, and T. Uhl. Hybrid modelling of an urban bus. *Mechanics and Control*, 32(1):13–20, 2013.
[27] A. Kozanecka. Solaris nT18 ATM Milano. Technical Report 52/2019, Homologation and Test Department, Solaris Bus & Coach S.A., Bolechowo, 2019.
[28] K. Kural, P. Hatzidimitris, N. van de Wouw, I. Besselink, and H. Nijmeijer. Active trailer steering control for high-capacity vehicle combinations. *IEEE Trans. Intell. Vehicles*, 2(4):251–265, 2017.
[29] J. P. Laumond. Controllability of a multibody mobile robot. *IEEE Trans. on Robotics and Automation*, 9(6):755–763, 1993.
[30] G. Leduc. Longer and Heavier Vehicles. An overview of technical aspects. Technical Report EUR 23949 EN, Joint Research Centre, Institute for Prospective Technological Studies, Luxembourg, 2009.
[31] L. Ljung. *System Identification: Theory for the User (2nd Edition)*. Prentice Hall PTR, Upper Saddle River, New Jersey, 1999.
[32] O. Ljungqvist, N. Evestedt, D. Axehill, M. Cirillo, and H. Pettersson. A path planning and path-following control framework for a general 2-trailer with a car-like tractor. *J. Field Rob.*, 36(8):1345–1377, 2019.
[33] M.M. Michałek. Agile maneuvering with intelligent articulated vehicles: a control perspective. *IFAC PapersOnLine*, 52(8):458–473, 2019.
[34] M.M. Michałek. Modular approach to compact low-speed kinematic modelling of multi-articulated urban buses for motion algorithmization purposes. In *2019 IEEE IVS*, pages 1803–1808, Paris,France, 2019.
[35] H. Montes, C. Salinas, R. Fernandez, and M. Armada. An experimental platform for autonomous bus development. *Appl. Sci.*, 7(1131):1–22, 2017.
[36] M. Murtagh, J. Early, G. Stevens, G. Cunningham, and R. Douglas. Modelling and control of a hybrid urban bus. *SAE Technical Paper*, 2019-01-0354:1–11, 2019.
[37] R. Orosco-Guerrero, E. Aranda-Bricaire, and M. Velasco-Villa. Modeling and dynamic feedback linearization of a multi-steered N-trailer. In *IFAC 15th Triennial World Congress*, 2002.
[38] P. Polack, F. Altche, B. d'Andrea Novel, and A. de La Fortelle. The kinematic bicycle model: a consistent model for planning feasible trajectories for autonomous vehicles? In *2017 IEEE IVS*, pages 812–818, Redondo Beach, USA, 2017.
[39] R. Rajamani. *Vehicle dynamics and control. 2nd Edition*. Springer, 2012.
[40] P. Rouchon, M. Fliess, J. Levine, and P. Martin. Flatness, motion planning and trailer systems. In *Proceedings of the 32nd Conference on Decision and Control*, pages 2700–2705, San Antonio, Texas, 1993.
[41] J. Schoukens and L. Ljung. Nonlinear system identification. A user-oriented road map. *IEEE Control Systems*, 36(6):28–99, 2019.
[42] X. Tian, R. He, X. Sun, Y. Cai, and Y. Xu. An ANFIS-based ECMS for energy optimization of parallel hybrid electric bus. *IEEE TVT*, 2019. DOI:10.1109/TVT.2019.2960593.
[43] D. Tilbury, O. J. Sørdalen, L. Bushnell, and S. S. Sastry. A multisteering trailer system: conversion into chained form using dynamic feedback. *IEEE Trans. on Robotics and Automation*, 11(6):807–818, 1995.
[44] Y. Zhang, A. Khajepour, and Y. Huang. Multi-axle/articulated bus dynamics modeling: a reconfigurable approach. *Vehicle System Dynamics*, 56(9):1315–1343, 2018.

Maciej Marcin Michałek (M'09, SM'16) received the Ph.D. and D.Sc. (habilitation) degrees in the field of automation and robotics from the Poznan University of Technology (PUT), Poland, in 2006, and 2015, respectively. He is currently an Associate Professor of PUT in the Institute of Automatic Control and Robotics. His current research concerns the modelling and control design problems for the nonholonomic systems, especially for mobile robots, N-trailer structures, and intelligent/automated vehicles. In years 2011-2019 he was an editorial board member of the *Journal of Intelligent & Robotic Systems*, and currently he serves as an associate editor for the *Journal of the Franklin Institute*. Publications of Dr. Michałek can be found at `maciej.michalek.pracownik.put.poznan.pl`.

Bartosz Patkowski graduated the Automatic Control and Robotics Engineering and received the M.Sc. degree from the Poznan University of Technology in 2017. Since 2017, he has been a specialist in the Solaris Bus & Coach (SBC) company in the areas of traction battery systems and advanced driver-assistance systems of the electric buses. He works as a Design Engineer in the Research and Development Department of SBC.

Tomasz Gawron (M'17) received the Ph.D. degree in the field of automation and robotics from the Poznan University of Technology (PUT), Poland, in 2019. He is currently a Research Assistant in the Institute of Automatic Control and Robotics, PUT. His current research is focused on motion planning and control of mobile robots, as well as program synthesis for robotic systems.